Structural Engineering and Mechanics, *Vol. 71, No. 1 (2019) 65-75*
DOI: https://doi.org/10.12989/sem.2019.71.1.065

Dynamic fracture instability in brittle materials: Insights from DEM simulations

Miaomiao Kou[1,4], Dongchen Han[1,2], Congcong Xiao[3] and Yunteng Wang*[4]

[1]School of Civil Engineering, Qingdao University of Technology, Qingdao, 266033, China
[2]Institute of Qingdao, Ernst & Young, Qingdao, 266000, China
[3]China Resources Land Ltd., Shanghai, 201206, China
[4]Cooperative Innovation Center of Engineering Construction and Safety in Shandong Blue Economic Zone, Qingdao, 266033, China

(Received January 14, 2019, Revised March 14, 2019, Accepted March 20, 2019)

Abstract. In this article, the dynamic fracture instability characteristics, including dynamic crack propagation and crack branching, in PMMA brittle solids under dynamic loading are investigated using the discrete element method (DEM) simulations. The microscopic parameters in DEM are first calibrated using the comparison with the previous experimental results not only in the field of qualitative analysis, but also in the field of quantitative analysis. The calibrating process illustrates that the selected microscopic parameters in DEM are suitable to effectively and accurately simulate dynamic fracture process in PMMA brittle solids subjected to dynamic loads. The typical dynamic fracture behaviors of solids under dynamic loading are then reproduced by DEM. Compared with the previous experimental and numerical results, the present numerical results are in good agreement with the existing ones not only in the field of qualitative analysis, but also in the field of quantitative analysis. Furthermore, effects of dynamic loading magnitude, offset distance of the initial crack and initial crack length on dynamic fracture behaviors are numerically discussed.

Keywords: dynamic fracture instability; crack propagation; crack branching; brittle solids; discrete element method

1. Introduction

The dynamic fracture problems in brittle solids is an interesting phenomena (Bowden and Brunton 1967; Ravi-Chandar and Knauss 1984; Fineberg *et al*. 1991; Rosakis *et al*. 1999), including crack propagation, crack bifurcation, crack branching, crack-path instability, successive branching, secondary or circumferential cracking, asymmetries of crack growth paths, etc., in the experiments attract large attentions from scholars (Bowden and Brunton 1967; Ravi-Chandar and Knauss 1984; Fineberg *et al*. 1991; Sharon *et al*. 1995; Fineberg and Marder 1999; Sharon and Fineberg 1999; Rabczuk *et al*. 2009; Fineberg and Bouchbinder 2015). In this interesting problems, the emergence of a critical crack tip speed of dynamic fracture process in brittle solids shows the dramatical increase of the fracture energy dissipation. For example, the saturation in crack speed affects the parasitic microcracks which emerge at an angle to the main crack. Ravi-Chandar and Knauss (1984) attributed the phenomenon of dynamic crack growth instability, i.e., crack propagation and crack branching, in brittle solids to microstructural defects of the fracture zone ahead of the crack tip, in which nucleation, growth and coalescence of voids take place. Furthermore, Ravi-Chandar and Knauss (1984), Fineberg *et al*. (1991) found that the evolution of these processes and the microscopic path instabilities provide a rate- and state-dependent characteristics to dynamic fracture energy in the laboratory tests. However, the aforementioned the experimental studies are restricted by the monitoring techniques, which is difficult to reveal the mechanism of dynamic fracture instabilities in brittle solids.

In the past decades, three main types of numerical methods, including atomistic mechanics, continuoum mechanics and discontinuous mechanics, were applied to investigate the dynamic fracture characteristics of brittle solids (Cox *et al*. 2005; Buehler and Gao 2006; Fineberg and Bouchbinder 2015). In the aspect of atomistic mechanics, the Molecular Dynamic (MD) was applied to simulate and study crack propagation and crack branching in dynamic brittle fracture problems (Cox *et al*. 2005; Abraham 2005; Buehler and Gao 2006; Procaccia and Zylberg 2013; Bouchbinder *et al*. 2014). However, numerical methodologies on the basis of atomistic mechanics is computational time cost, which is not suitable to study the macroscopic dynamic fracture problems. In the aspect of continuum mechanics, the finite element method (FEM) is the most popular method to study dynamic fracture problems. Some scholars have successfully applied FEM and extended FEM to simulate the dynamic fracture behaviors (Belytschko *et al*. 2003; Song *et al*. 2008; Song and Belytschko 2009; Yang *et al*. 2015; Meng and Wang 2015). However, to simulate dynamic crack growth, the additional techniques, such as mesh remeshing technique, element-erosion technique, cohesive zone technique, etc., and additional branching failure criteria are required to be added into the standard FEM, which results in the difficulties of simulating dynamic fracture phenomena (Song *et al*. 2008). For sake of easily simulating fracture phenomena in brittle solids, peridynamics (Shojaei *et al*. 2016, 2018, 2019; Zaccariotto *et al*. 2018; Bazazzadeh *et al*.

*Corresponding author, Ph.D.
E-mail: wytcqu2014@126.com

http://www.techno-press.com/journals/sem&subpage=7
ISSN: 1225-4568 (Print), 1598-6217 (Online)

2019a, b) and phase-field model (Miehe *et al*. 2010a, b, Zhang *et al*. 2018, Emdadi *et al*. 2018, Carlsson and Isaksson 2019) were proposed based the continuous mechanics (Sarkar *et al*. 2017, Nowruzpour and Reddy 2018, Nowruzpour *et al*. 2019).

The discrete element method (DEM) (Potyondy and Cundall 1998, 2004) is a powerful numerical method based on discontinuous mechanics and is initially proposed for predicting the behaviors of particulate media. This numerical methodology is popular and natural technique to study the dynamic fracture behaviors of granular geomaterials (Potyondy and Cundall 1998, 2004, Cho *et al*. 2007, Mohammed *et al*. 2015, Sarfarazi and Haeri 2018, Haeri *et al*. 2018a, b, c, d, e, Cao *et al*. 2016, 2018a, b, c) and powders (Martin *et al*. 2006, Hedjazi *et al*. 2012, Meng *et al*. 2018). The most feature of DEM is that the method consists in describing materials as an assembly of local interacting material particles. The motion of particles within the framework of DEM obey Newton's second law, in which displacements and rotations are updated at the transient suitable time increment (Potyondy and Cundall 2004, Martin *et al*. 2003, 2006, Hedjazi *et al*. 2012). In the whole DEM system, a state path evolves to follow the conditions that enforce force equilibrium at every material particles. The boundary conditions can be implemented using rigid geometric objects such as cylinders, planes, spheres or periodic boundary conditions. The local interactions between material particles are described using the suitable contact law, including the linear elastic laws coupled with Coulomb friction. The second characteristic of DEM is that the DEM allows material particles bonding so that tensile forces and resisting moments are transmitted through contacts (Potyondy and Cundall 1998, 2004, Cho *et al*. 2007, Mohammed *et al*. 2015, Sarfarazi and Haeri 2018, Haeri *et al*. 2018a, b, c, d, e, Cao *et al*. 2016, 2018a, b, c). Since the DEM is suitable to simulate failure process of geomaterials, there is rare studies on dynamic fracture problems using DEM (Hedjazi *et al*. 2012, Braun and Fernandez-Saez 2014, Kosteski *et al*. 2012).

DEM is applied to investigate the dynamic failure behaviors of brittle solids subjected to dynamic loads. The crack propagation and crack branching in brittle PMMA plate with a single pre-existing crack is firstly reproduced by DEM. Moreover, the numerical predicted terminal crack speeds attained in PMMA specimens are substantially lower than the Rayleigh wave speed and the computed crack speeds agree quite well with the reported experimental and numerical results not only in the field of quantitative analysis, but also in the field of qualitative analysis. The quantitative and qualitative comparisons with the existing experimental data illustrate the effectiveness and accuracy of the microscopic parameters in DEM simulations. Meanwhile, the microscopic parameters for PMMA materials in DEM are calibrated using the above quantitative and qualitative analysis. Furthermore, the influences of dynamic loading magnitude, offset distance of the initial crack and initial crack length on dynamic fracture behaviors, including dynamic fracture patterns and critical crack propagation speed in brittle solids under dynamic loading are numerically investigated.

The present article is structured as follows. In Section 2, we briefly describe the DEM theory. In Section 3, the microscopic parameters of DEM for PMMA material are calibrated, and numerical reproduction of dynamic fracture process in brittle solids under dynamic loading are shown. In Section 4, influences of loading parameters and geometrical parameters on dynamic fracture features are investigated and discussed. Conclusions are drawn in Section 5.

2. Numerical methodology

In the discrete element method (DEM), the dense materials are represented by a packing of overlapping nearly monosized spherical particles, which was proposed by Potyondy and Cundall (1998, 2004) and Cho *et al*. (2007). To simulate the tensile fracture and shear fracture characteristics of brittle solids under different loading conditions, the parallel bond DEM was proposed by Cho *et al*. (2007), which has been widely used to simulate complicated fracture behaviors of brittle solids (Mohammed *et al*. 2015, Sarfarazi and Haeri 2018, Haeri *et al*. 2018a, b, c, d, e, Cao *et al*. 2016, 2018a, b, c).

In the parallel bond DEM, the intact brittle solids is represented by a composite of separate particles bonded together. There are two different contact interactions named as normal bonds and tangential bonds based on the deformation characteristics of separated particles. The two different bonds provide the normal and shear stiffness between adjacent interacting particles. In addition, there are two different sets of contact springs bonded among particles. The parallel bond DEM approximates the mechanical behaviors of brittle and quasi-brittle connecting the two adjacent particles, which acts like a beam resisting the moment induced by the particle rotation or shearing within the bonded region (Potyondy and Cundall 1998, 2004, Cho *et al*. 2007, Mohammed *et al*. 2015, Sarfarazi and Haeri 2018, Haeri *et al*. 2018a, b, c, d, e, Cao *et al*. 2016, 2018a, b, c). According to the remarks by Cho *et al*. (2007), the parallel bond DEM is a more realistic bond model for brittle and quasi-brittle materials whereby the bonds may break in either tension or shearing with an associated reduction in stiffness (Cho *et al*. 2007). Based on the previous studies (Potyondy and Cundall 1998, 2004, Cho *et al*. 2007, Mohammed *et al*. 2015, Sarfarazi and Haeri 2018), the first set of springs between two adjacent particles is belong to grain behaviors providing normal and shear stiffness k_N and k_T, respectively. While, the second set of springs between two adjacent particles is belong to bond behaviors providing the parallel bond normal and shear stiffness $\overline{k}_N$ and $\overline{k}_T$, which are uniformly distributed over a disc shaped cross section lying on the contact plane.

The normal and shear stiffness representing the material mechanical behaviors between two adjacent particles can be expressed as

$$k_N = 2hE_c \tag{1}$$

$$k_T = \frac{k_N}{k_N/k_T} \tag{2}$$

where $h = 1$ is the thickness for two-dimensional cases; E_c denotes Young's modulus of the particle; k_N/k_T is designated as the ratio of normal to shear stiffness of the particle.

The normal and shear stiffness of parallel bond between two interacting material particles are assigned as

$$\overline{k}_N = \frac{\overline{E}_c}{\overline{R}} \tag{3}$$

$$\overline{k}_T = \frac{\overline{k}_T}{\overline{k}_N/\overline{k}_T} \tag{4}$$

in which $\overline{E}_c$ denotes the Young's modulus of the parallel bond; $\overline{R}$ is the equivalent radius of two interacting discrete particles; and $\overline{k}_N/\overline{k}_T$ represents the ratio of normal to shear stiffness of the parallel bond.

The equivalent radius between two interacting discrete particles is related to radii of two interacting discrete particles, i.e., R_1 and R_2 and thickness of corresponding normal or shear bonds, i.e., h_b. The equivalent radius can be written as

$$\overline{R} = \frac{R_1 R_2}{R_1 + R_1 - h_b} \tag{5}$$

For simplification, the thickness of associated normalized or shear bonds is adopted to be zero in this article. The normal and shear bond radius is assumed as same, which is designated as a_b. In the present numerical simulations, the normalized bond radius a^* can be defined as

$$a^* = \frac{a_b}{2\overline{R}} \tag{6}$$

Forces on the normal and shear bonds connecting two interacting neighbor particles can be divided into the normal components, N, and the tangential components, T. The two kinds of forces act on the two spherical particles with equivalent radius $\overline{R}$ through the bonds can be expressed as

$$F_N = \overline{k}_N a^* \overline{R} u_N \tag{7}$$

$$F_T = -\overline{k}_T a^* \overline{R} u_T \tag{8}$$

in which u_N and u_T are the accumulated normal and tangential displacements integrated from the actual relative displacements of two interacting spherical particles. It should be noted that forces are taken as positive in tension, while the tangential force opposes the accumulated tangential displacements.

Furthermore, the bonded contacts between two interacting spherical particles can transmit resisting moments, i.e., M_N and M_T, along the normal and tangential directions, which can be written in the following forms.

$$M_N = -\overline{k}_T \left(a^* \overline{R}\right)^3 \vartheta_N \tag{9}$$

$$M_T = -\overline{k}_N \left(a^* \overline{R}\right)^3 \vartheta_T \tag{10}$$

where ϑ_N and ϑ_T are designated as the accumulated relative rotations of two interacting spherical particles along the normal and tangential directions. It should be noted that the centre to centre distance between two interacting spherical particles are distributed in the packing, the stiffness and resisting moments from one bond to another can be approximated as the same (Martin *et al*. 2003, 2006, Hedjazi *et al*. 2012). Thus, we impose that a^* is equal to 0.5 in this research. In the parallel bond DEM, the fracture criteria are included in the microscopic properties of the different bonds. When we approximate the solid bonds by a cylindrical beam of radius a_b and using the beam theory, the associated maximum tensile and shear stresses on the bond periphery can be evaluated as (Potyondy and Cundall 1998, 2004, Cho *et al*. 2007)

$$\sigma_N = \frac{F_N}{4\pi\left(a^* \overline{R}\right)^2} + \frac{|M_T|}{2\pi\left(a^* \overline{R}\right)^2} \tag{11}$$

$$\sigma_T = \frac{|F_T|}{4\pi\left(a^* \overline{R}\right)^2} + \frac{|M_N|}{2\pi\left(a^* \overline{R}\right)^2} \tag{12}$$

Therefore, the bond breakage may occur due to the tensile and shear deformation of the bond cylindrical beam. It is assumed that the following fracture criteria is adopted in this article.

$$\sigma_N > f_t \tag{13}$$

$$\sigma_T > f_\tau \tag{14}$$

in which f_t is the uniaxial tensile strength of brittle materials, and f_τ is the maximum shear strength of materials on the bonds.

The conventional explicit time integration in the DEM is adopted to conduct the numerical simulations of dynamic fracture phenomena in brittle solids under dynamic loading.

3. Microscopic calibration

To calibrate the microscopic parameters in the parallel bond DEM for brittle PMMA materials for dynamic fracture problems, a classical experimental test of PMMA plates under dynamic loading conditions is reproduced using the developed DEM. A thin rectangular plate with dimension of $0.1 \text{ m} \times 0.04 \text{ m}$ with a long horizontal pre-cracked under remote and symmetric tensile dynamic loading conditions as shown in Fig. 1(a). It can be found from Fig. 1(a) that the pre-existing edged crack with length of $a_0 = 0.05$ m is located at the center position along vertical direction with $h_0 = 0.02$ m. The sharp tensile dynamic loads are suddenly applied and keep constant. The sharp dynamic tensile loading of $\sigma(t) = 1.0$ MPa is symmetrically applied on the upper and bottom boundaries of the PMMA plate, as shown in Fig. 1(a). The macroscopic material parameters of

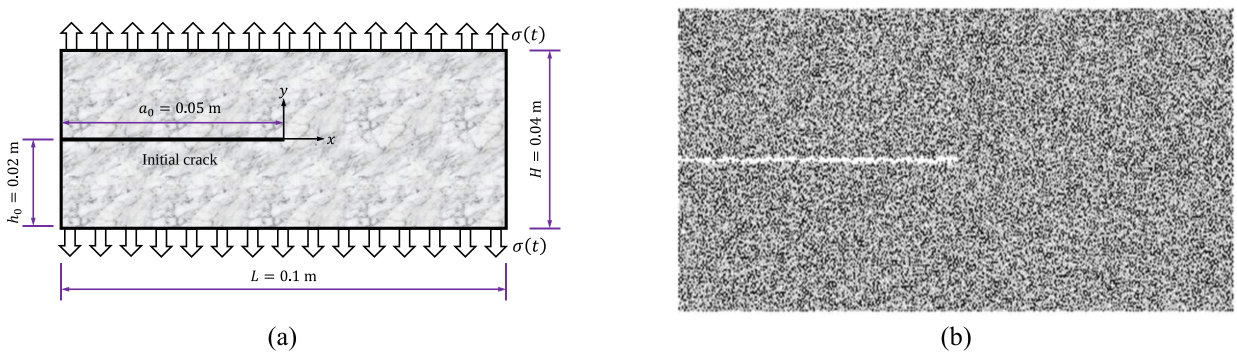

Fig. 1. The geometrical and loading conditions of a PMMA plate with a single initial crack: (a) schematics and (b) numerical specimen

Table 1 Experimental results for the macroscopic mechanical parameters of intact PMMA material

Mass density ρ (kg/m^3)	Young's modulus E (GPa)	Poisson's ratio υ	Uniaxial tensile strength f_t (MPa)
2,235	3.24	0.35	10.0

Table 2 Microscopic parameters for brittle PMMA materials in parallel bond DEM

Microscopic parameters	Values
Maximum particle radius, $R_{\max}$ (mm)	0.35
Minimum particle radius, $R_{\min}$ (mm)	0.15
Ratio of maximum to minimum radius of the particle, $R_{\max}/R_{\min}$	2.333
Particle contact modulus, E_c (GPa)	3.24
Ratio of normal to shear stiffness of the particle, k_N/k_T	1.8
Particle friction coefficient, μ	0.577
Parallel bond modulus, $\overline{E}_c$ (GPa)	3.24
Ratio of normal to shear stiffness of the parallel bond, f_t (MPa)	10
Parallel-bond normal strength, standard deviation, (MPa)	2
Parallel bond shear strengths, f_τ (MPa)	70
Parallel-bond shear strength, standard deviation, (MPa)	2

PMMA materials are same as ones listed in Table 1, and the same microscopic parameters in the parallel bond DEM are shown in Table 2 in the present numerical simulations.

In the parallel bond DEM numerical simulations, 42,586 discrete spherical particles with the maximum radius of $R_{\max} = 0.35$ mm and the minimum radius of $R_{\min} = 0.15$ mm are used to construct the thin brittle PMMA plate with an initial crack under dynamic loading, as shown in Fig. 1(b). The velocity Verlet-algorithm with time step size of $\Delta t = 1.0 \times 10^{-7}$ s is adopted to model the dynamic fracture process of brittle PMMA plates under dynamic loading conditions in this parallel bond DEM.

Fig. 2 shows the crack growth paths in the brittle plates with a single pre-existing crack under dynamic tensile loading conditions. During the dynamic fracture process, it can be found the when time is equal to 15 μs, a crack is initiated from the tip of the pre-existing crack and the emanating crack propagates along an approximate straight horizontal direction, as shown in Fig. 2(a). With increasing the dynamic tensile loading time, the cracks emanating from the tip of pre-existing crack continues to growth along the straight horizontal direction, as shown in Fig. 2(b) and Fig. 2(c). When the dynamic tensile loading time equates to about 30 μs, it can be found from Fig. 2(d) that the main straight crack emanating from the pre-existing crack tip is split into two macroscopic crack branches. As the dynamic tensile loads continue to apply on the upper and bottom boundaries of the brittle PMMA plate, the two macroscopic crack branches continue to growth along inclined directions, as shown in Fig. 2(e). Finally, it can be found from Fig. 2(f) that the two macroscopic crack branches continue to propagate separately towards the edge of the brittle PMMA plate.

The final predicted numerical crack growth paths in brittle PMMA plates with an initial crack under dynamic tensile loading are compared with the previous experimental observations (Bowden and Brunton 1967; Ravi-Chandar and Knauss 1984; Fineberg *et al*. 1991; Sharon *et al*. 1995; Fineberg and Marder 1999; Sharon and Fineberg 1999; Rabczuk *et al*. 2009; Fineberg and Bouchbinder 2015) and the previous numerical results (Song *et al*. 2008; Song and Belytschko 2009; Zhang and Chen 2014; Shojaei *et al*. 2018; Carlsson and Isaksson 2019), as shown in Fig. 3. This analysis also illustrates the microscopic parameters for brittle PMMA materials in the present parallel bond DEM are effective and accuracy in the field of qualitative analysis. In addition, the microscopic cracks can be captured in the macroscopic crack branches and main straight crack as same as the previous experimental observations (Bowden and Brunton 1967; Ravi-Chandar and Knauss 1984; Fineberg *et al*. 1991; Sharon *et al*. 1995; Fineberg and Marder 1999).

The crack propagation speed is an important indicator for dynamic crack propagation and one of the important topics in the theoretical studies and engineering application. Many researches indicated that the crack propagation speed has critical values. There is a critical crack propagation speed which has been commonly accepted (Bowden and Brunton 1967; Ravi-Chandar and Knauss 1984; Fineberg *et al*. 1991; Sharon *et al*. 1995; Fineberg and Marder 1999; Sharon and Fineberg 1999; Rabczuk *et al*. 2009; Song *et al*. 2008; Song and Belytschko 2009; Zhang and Chen 2014;

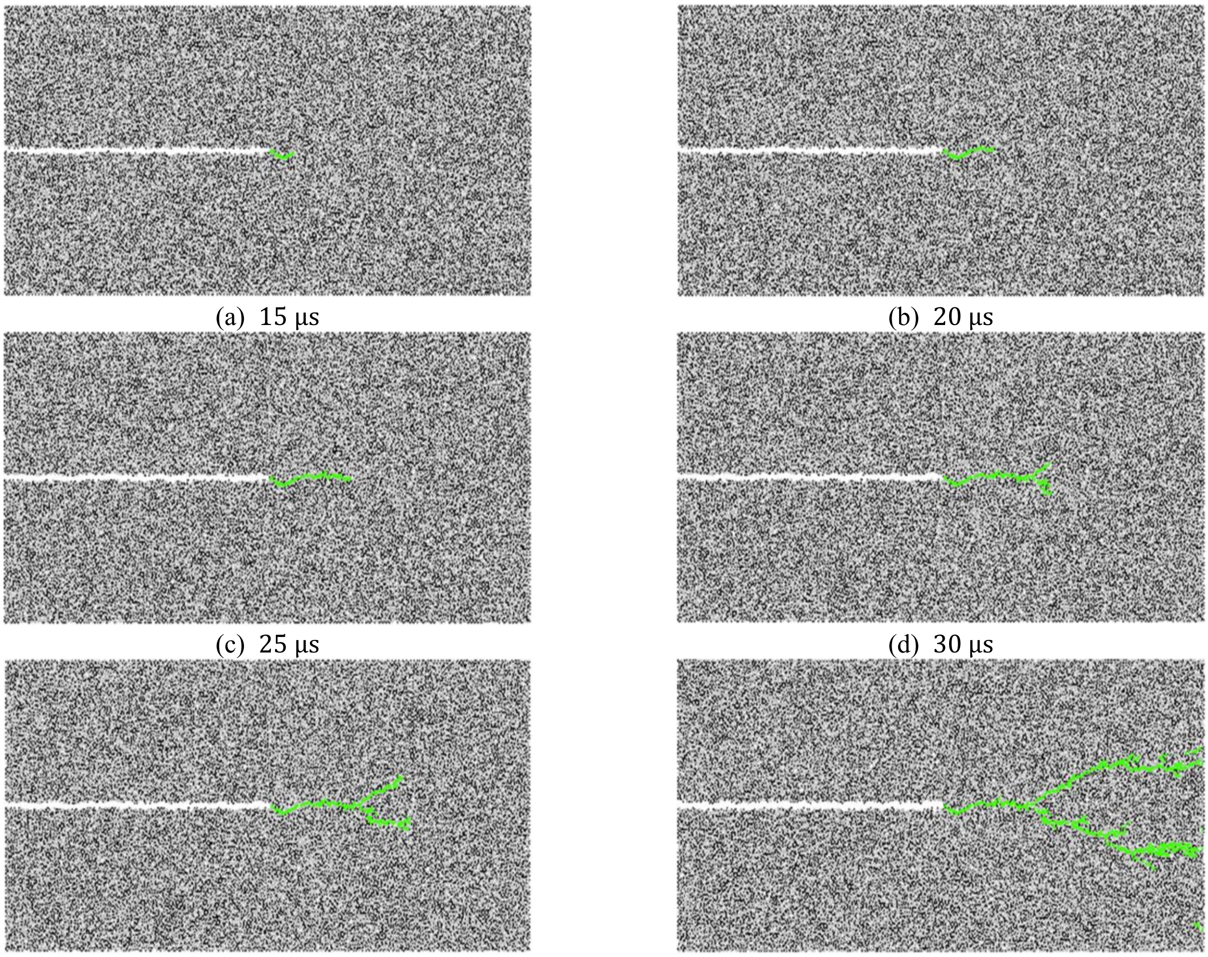

(a) 15 μs (b) 20 μs
(c) 25 μs (d) 30 μs
(e) 35 μs (f) 45 μs

Fig. 2 The process of crack propagation and crack branching in the PMMA plate with an initial crack under dynamic loading

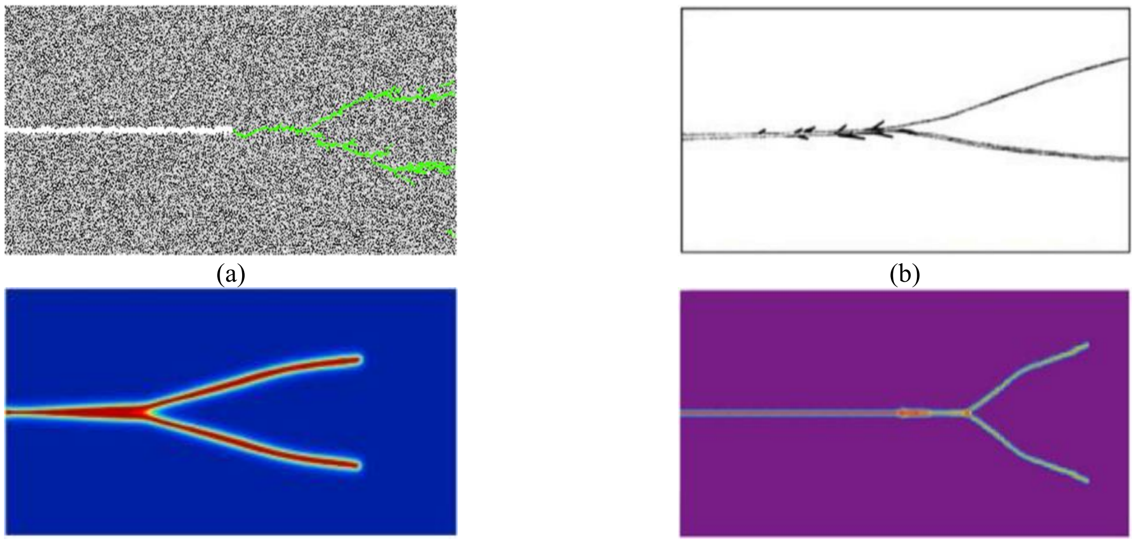

(a) (b)
(c) (d)

Fig. 3 Comparison of dynamic cracking patterns obtained from (a) the present numerical simulation, (b) the previous experimental observation (Ravi-Chandar and Knauss 1984), (c) the phase field model results (Carlsson and Isaksson 2019), (d) the adaptive multi-grid peridynamic results (Shojaei *et al*. 2018)

Shojaei *et al*. 2018; Carlsson and Isaksson 2019; Fineberg and Bouchbinder 2015). Based on the previous studies, the phenomena of crack branching occurs in brittle PMMA materials accompanies by a drop in crack tip velocity after the crack tip propagation speed achieves a maximum value.

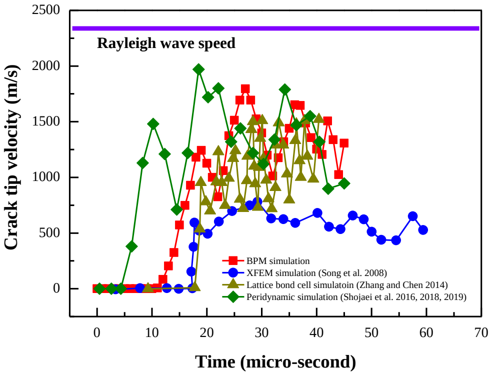

Fig. 4 Crack tip propagation speed predicted from different numerical methodologies

Fig. 4 shows that the crack tip velocity profiles also are very close to the numerical results obtained by the XFEM (Song *et al*. 2008; Song and Belytschko 2009), lattice bond cell simulation (Zhang and Chen 2014) and bond-based peridynamics (Shojaei *et al*. 2016, 2018, 2019). The numerically predicted crack tip velocity are in good agreement with the previous experimental results, which demonstrate the microscopic parameters in the parallel bond DEM are effective and accuracy in the field of quantitative analysis under dynamic tensile loading.

It can be found from Fig. 4 that once the crack starts to propagate, the crack propagation speed gradually increases to its maximum value of 1753 m/s at about 28.8 μs. After crack propagation speed reaches its maximum value at about 28.8 μs, the macroscopic crack branches happen and the main macroscopic straight crack splits into two macroscopic crack branches. As shown in Fig. 4, the maximum crack tip velocity obtained from the present parallel bond DEM simulations are less than the Rayleigh wave speed, which conforms to the previous experimental results (Bowden and Brunton 1967). Based on the aforementioned qualitative and quantitative studies on the brittle PMMA plate with a pre-existing crack under dynamic tensile loading conditions, the present numerical microscopic parameters is also suitable to simulate the fracture behaviors of brittle PMMA materials not only in the field of qualitative analysis, but also in the field of quantitative analysis.

4. Numerical results and discussions

The effect of dynamic loading magnitudes, offset distances and initial crack lengths on the dynamic fracture behaviors of brittle PMMA materials are discussed in this section.

4.1 Effect of dynamic loading magnitudes

In this subsection, effect of dynamic loading magnitudes on dynamic fracture characteristics of brittle PMMA materials are numerically investigated using four numerical PMMA plates subjected to sharp dynamic loads with four different magnitudes of $\sigma_0 = 1.00$ MPa, $\sigma_0 = 1.25$ MPa, $\sigma_0 = 1.50$ MPa and $\sigma_0 = 1.75$ MPa. The microscopic parameters in the parallel bond DEM simulations and time integrations scheme are same as ones in Section 4.

The numerically predicted ultimate crack growth paths in the above four numerical brittle PMMA plates under different dynamic tensile loading conditions are plotted in Fig. 5. It can be found from Fig. 5(a) that the crack growth paths are approximate symmetrical. The microscopic cracks occur at the surfaces of two macroscopic crack branches and the main straight crack, as shown in Fig. 5(a). It can be found from Fig. 5(b) that the first crack branching point in the brittle PMMA plate under dynamic $\sigma_0 = 1.00$ MPa is same at the one in brittle the brittle PMMA plate under dynamic $\sigma_0 = 1.25$ MPa. When the dynamic tensile loading magnitude is equal to $\sigma_0 = 1.25$ MPa, the secondary macroscopic branches occur at the brittle PMMA plate, as shown in Fig. 5(b). As the dynamic tensile loading magnitude increase to $\sigma_0 = 1.50$ MPa, the macroscopic crack branching occurs earlier than ones under low dynamic loading magnitudes, i.e., $\sigma_0 = 1.00$ MPa and $\sigma_0 = 1.25$ MPa, as shown in Fig. 5(c). It can also be observed from Fig. 5(c) that the multiple crack branches happens in the brittle PMMA plates under dynamic tensile loading magnitude of $\sigma_0 = 1.50$ MPa. Similar complicated crack branches can also be observed in the ultimate crack paths in the brittle PMMA plate under dynamic tensile loading with magnitude of $\sigma_0 = 1.75$ MPa, as shown in Fig. 5(d). Under the high dynamic loading conditions, the multiple crack branches in the brittle PMMA plates lead to the asymmetrical final crack growth paths, as shown in Fig. 5(c)-Fig. 5(d). It can be observed from Fig. 5 that the crack branching occurs much earlier in brittle PMMA plates under low dynamic tensile loading than that in brittle PMMA plates subjected to high dynamic tensile loads.

The evolutions of crack tip velocities in the aforementioned four brittle PMMA plates under various dynamic tensile loading conditions are depicted in Fig. 6. It can be found from Fig. 6 that the crack propagation speed profiles in different brittle PMMA plates shows similar shapes. As the dynamic tensile loads increases, it can also be observed from Fig. 6 that the maximum crack tip velocity slightly increases in the brittle PMMA plates. Moreover, the maximum crack tip velocities in above four different brittle PMMA plates are smaller than the Rayleigh wave speed, which obeys the experimental remarks (Bowden *et al.* 1967; Ravi-Chandar and Knauss 1984; Fineberg *et al*. 1991), as shown in Fig. 6

5.2 Effect of offset distances

To study the effect of the pre-existing crack offset distances on dynamic fracture characteristics of brittle PMMA materials under dynamic tensile loading conditions, six different numerical PMMA plates with different offset distances are simulated in the framework of parallel bond DEM. The six different offset distances of initial cracks are listed as follows: $h_0 = 0.02$ m, $h_0 = 0.016$ m, $h_0 = 0.012$ m, $h_0 = 0.008$ m, $h_0 = 0.006$ m and $h_0 = 0.004$ m. The microscopic parameters in the parallel bond DEM simulations and time integrations scheme are same as ones in Section 4. The dynamic tensile loading magnitudes of the above six brittle PMMA plates are fixed as $\sigma_0 = 1.0$ MPa.

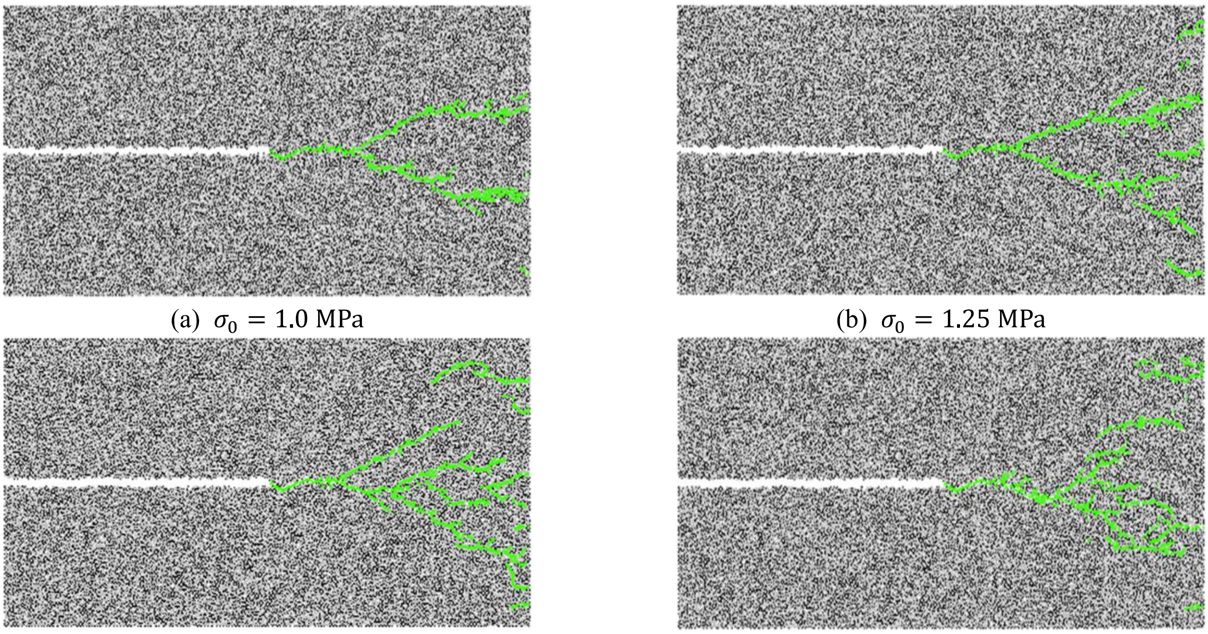

(a) $\sigma_0 = 1.0$ MPa (b) $\sigma_0 = 1.25$ MPa

(c) $\sigma_0 = 1.50$ MPa (d) $\sigma_0 = 1.75$ MPa

Fig. 5 Influence of dynamic loading magnitudes on dynamic fracture patterns in PMMA solids under dynamic loading

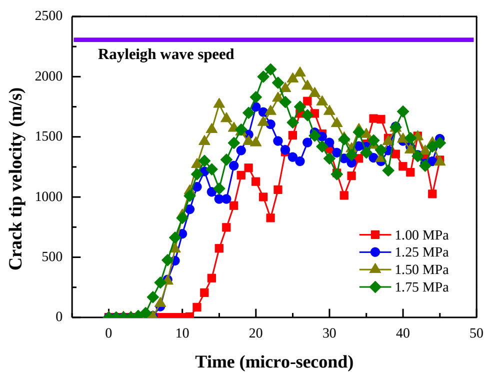

Fig. 6 Influence of dynamic loading magnitudes on crack tip propagation speed in PMMA solids under dynamic loading

The numerically predicted ultimate crack growth paths in the above six numerical brittle PMMA plates with various offset distances under dynamic tensile loading condition of $\sigma_0 = 1.0$ MPa are plotted in Fig. 7. It can be found from Fig. 9(a) that the crack growth paths are approximate symmetrical in the brittle PMMA plate with a single pre-existing crack of $h_0 = 0.02$ m. The microscopic cracks occur at the surfaces of two macroscopic crack branches and the main straight crack, as shown in Fig. 7(a). When the offset distance of the single initial crack is equal to $h_0 = 0.016$ m, the secondary crack branches occur near the right boundary of the brittle PMMA plates during the dynamic cracking process, as shown in Fig. 7(b). Meanwhile, it can be observed from Fig. 7(a)-7(b) that the microscopic cracks are initiated at the surfaces of main straight crack and macroscopic crack branches. When the offset distance of an initiate crack changes from $h_0 = 0.012$ m to $h_0 = 0.008$ m, the crack branching patterns in brittle PMMA plates under dynamic tensile loading become much more complicated, and the trajectories of the main cracks become curvier, as shown in Fig. 7(c)-7(d). Furthermore, it can also observed from Fig. 7(a)-Fig. 7(f) that main cracks propagate towards the middle horizontal line along the more bent trajectories as the offset distance of initial crack varies from $h_0 = 0.02$ m to $h_0 = 0.004$ m. In addition, when the offset distance of initial crack equates to $h_0 = 0.006$ m or $h_0 = 0.004$ m, the macroscopic crack branches also propagate along the curve trajectories towards the middle horizontal lines in the brittle PMMA plates under dynamic tensile loading conditions, as shown in Fig. 7.

The variations of maximum crack tip velocity in the brittle PMMA plates with the various pre-existing crack offset distances under dynamic tensile loading condition of $\sigma_0 = 1.0$ MPa are plotted in Fig. 8. It can be observed from Fig. 8 that when the offset distance of initial crack in the brittle PMMA plates increases from 0 mm to 8 mm, the maximum crack tip velocity during the dynamic fracturing process in the brittle PMMA plates decreases from about 1658 m/s to approximate 1475 m/s, which are less than the Rayleigh wave speed. Furthermore, when the offset distance of initial crack in the brittle PMMA plates increases from 8 mm to 16 mm, the maximum crack tip velocity during the dynamic fracturing process in the brittle PMMA plates decreases from approximate 1475 m/s to about 1612 m/s, as shown in Fig. 8.

5.3 Effect of initial crack length

To study the effect of the initial crack length on dynamic fracture characteristics of brittle PMMA materials under dynamic tensile loading conditions, four different numerical

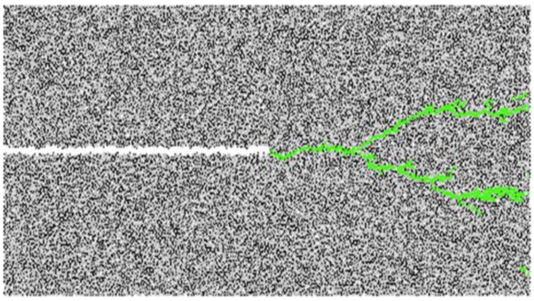

(a) $h_0 = 0.02$ m

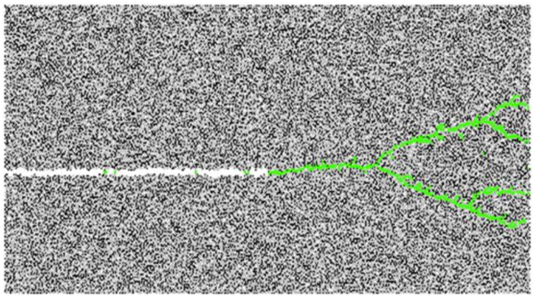

(b) $h_0 = 0.016$ m

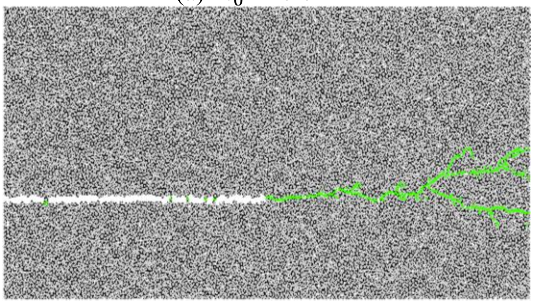

(c) $h_0 = 0.012$ m

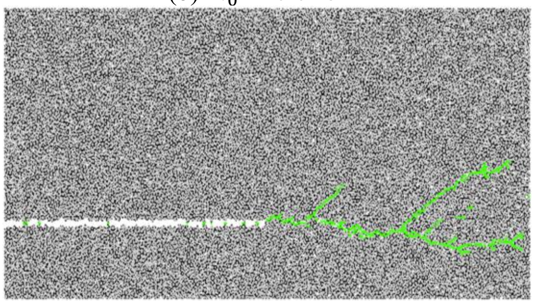

(d) $h_0 = 0.008$ m

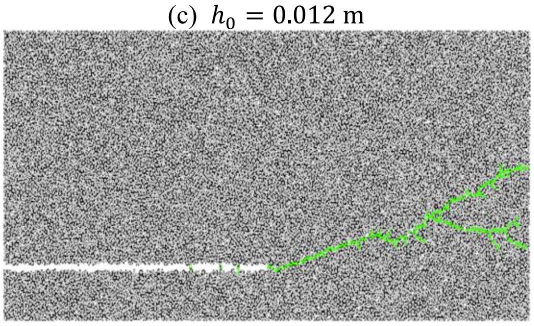

(e) $h_0 = 0.006$ m

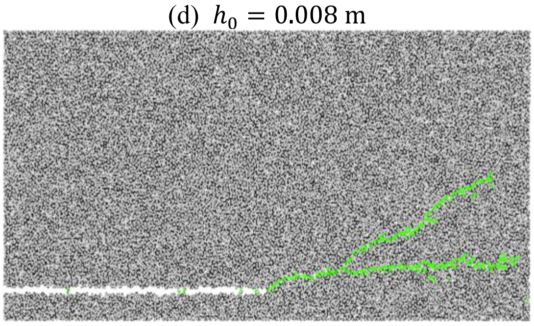

(f) $h_0 = 0.004$ m

Fig. 7 Influence of offset distances on dynamic fracture patterns in PMMA solids under dynamic loading

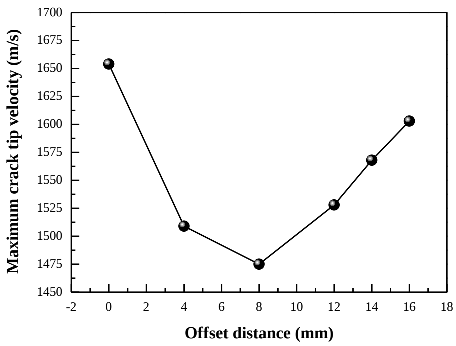

Fig. 8 Influence of offset distances on maximum crack tip velocity in PMMA solids under dynamic loading

PMMA plates with various initial crack lengths are modeled in the parallel bond DEM framework. The four different initial crack lengths in the brittle PMMA plates are listed as follows: $a_0 = 50$ mm, $a_0 = 40$ mm, $a_0 = 30$ mm and $a_0 = 20$ mm. The microscopic parameters in the parallel bond DEM simulations and time integrations scheme are same as ones in Section 4. The dynamic tensile loading magnitudes of the above four brittle PMMA plates are fixed as $\sigma_0 = 1.0$ MPa.

The numerically predicted ultimate crack growth paths in the above four numerical brittle PMMA plates with different initial crack lengths under dynamic tensile loading conditions are plotted in Fig. 9. It can be found from Fig. 9(a) that the crack growth paths are approximate symmetrical in the brittle PMMA plate with a single pre-existing crack of $a_0 = 50$ mm. The microscopic cracks occur at the surfaces of two macroscopic crack branches and the main straight crack, as shown in Fig. 9(a). When the initial crack length in brittle PMMA plates is equal to $a_0 = 40$ mm, not only the microscopic cracks happen at the surfaces of the main straight crack and macroscopic crack branches, and the secondary crack branches occur during the dynamic cracking process in the brittle PMMA plate under dynamic tensile loading, as shown in Fig. 9(b). It can be observed from Fig. 9(a) and Fig. 9(b) that length of the main straight crack in the brittle PMMA plate with $a_0 = 40$ mm is longer than that in the brittle PMMA plate with $a_0 = 50$ mm. With decreasing the initial crack length in brittle PMMA plates from $a_0 = 50$ mm to $a_0 = 20$ mm, the microscopic crack branches are much easier to occur in the brittle PMMA plates under dynamic tensile loading, as shown in Fig. 9(c)-9(d). The occurrence of macroscopic and microscopic branches in the brittle PMMA plates results in the asymmetrical crack growth paths during the dynamic

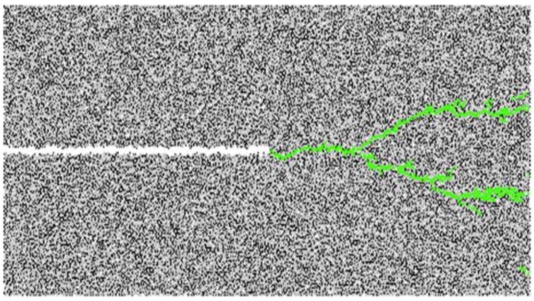

(a) $a_0 = 50$ mm

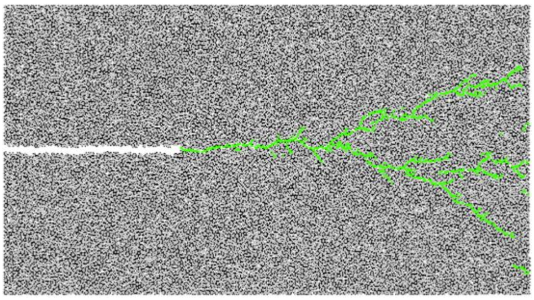

(b) $a_0 = 40$ mm

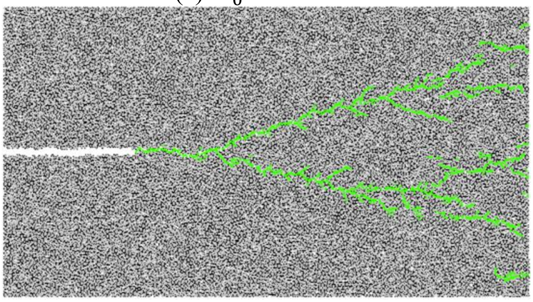

(c) $a_0 = 30$ mm

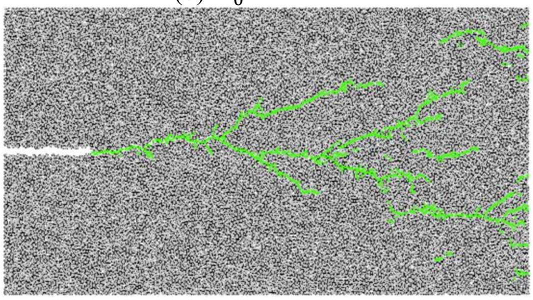

(d) $a_0 = 20$ mm

Fig. 9 Influence of initial crack lengths on dynamic fracture patterns in PMMA solids under dynamic loading

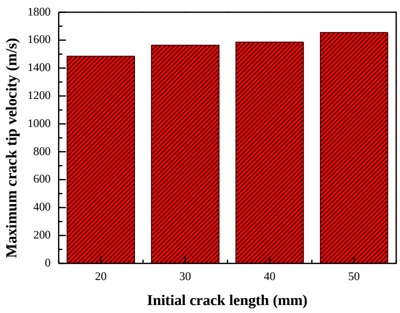

Fig. 10 Influence of initial crack length on maximum crack tip velocity in PMMA solids under dynamic loading

fracturing process, as shown in Fig. 9. In addition, it can also be observed from Fig. 9 that the main straight crack lengths decreases as the initial crack lengths in brittle PMMA plates decrease.

The variations of maximum crack tip velocity in the brittle PMMA plates with different initial cracks are plotted in Fig. 10. It can be observed from Fig. 10 that as the initial crack length in brittle PMMA plates under dynamic tensile loading conditions increases, the maximum value of crack tip velocity increases.

5. Conclusions

In this study, the insights of dynamic failure behaviors of brittle solids under dynamic loading conditions are numerically captured using the developed discrete element methodology (DEM). The microscopic parameters are first calibrated using the comparison between experimental data and the present numerical results. From the numerical analysis, the calibrating microscopic parameters selected in parallel bond DEM are effective and accurate in the simulations of brittle PMMA materials under dynamic loading conditions. Compared with the previous experimental and numerical results, the present numerical results are in good agreement with the existing ones not only in the field of qualitative analysis, but also in the field of quantitative analysis. Then, effects of dynamic loading magnitudes, pre-existing crack offset distances, and initial crack length on dynamic fracture behaviors, such as dynamic fracture patterns and critical crack propagation speed in brittle PMMA solids subjected to dynamic loads discussed.

Acknowledgments

This work was supported by Graduate Scientific Research and Innovation foundation of Chongqing, China (Grant No. CYB16012).

References

Abraham, F. (2005), “Unstable crack motion is predictable”, *J. Mech. Phys. Solids*, **53**(5), 1071-1078. https://doi.org/10.1016/j.jmps.2004.12.005.

Bazazzadeh, S., Shojaei, A., Zaccariotto, M. and Galvanetto, U. (2019a), “Application of the peridynamic differential operator to the solution of sloshing problems in tanks”, *Eng. Computations,* **36**(1), 45-83. https://doi.org/10.1108/EC-12-2017-0520.

Bazazzadeh, S., Zaccariotto, M. and Galvanetto, U. (2019b), “Fatigue degradation strategies to simulate crack propagation using peridynamic based computational methods”, *Lat. Am. J. Solids Struct.,* **16**(2). http://dx.doi.org/10.1590/1679-78255022.

Belytschko, T., Chen, H., Xu, J. and Zi, G. (2003), “Dynamic crack propagation based on loss of hyperbolicity and a new discontinuous enrichment”, *Int. J. Numer. Methods Eng.*,

58(12), 1873-1905. https://doi.org/10.1002/nme.941.

Bowden, F.P., Brunton, J.H., Field, J.E. and Heyes, A.D. (1967), "Controlled fracture of brittle solids and interruption of electrical current", *Nature*, **216**, 38-42.

Braun, M. and Fernandez-Saez, J. (2014), "A new 2D discrete model applied to dynamic crack propagation in brittle materials", *Int. J. Solids Struct.*, **51**(21-22), 3787-3797. https://doi.org/10.1016/j.ijsolstr.2014.07.014.

Buehler, M.J. and Gao, H. (2006), "Dynamic fracture instabilities due to local hyperelasticity at crack tips", *Nature*, **439**, 307-310.

Cao, R.H., Cao, P., Lin, H., Pu, C.Z. and Ou, K. (2016), "Mechanical behavior of brittle rock-like specimens with pre-existing fissures under uniaxial loading: Experimental studies and particle mechanics approach", *Rock Mech. Rock Eng.*, **49**(3), 763-783. https://doi.org/10.1007/s00603-015-0779-x.

Cao, R.H., Cao, P., Lin, H., Ma, G.W. and Chen, Y. (2018a), "Failure characteristics of intermittent fissures under a compressive-shear test: Experimental and numerical analyses", *Theor. Appl. Fract. Mech.*, **96**, 740-757. https://doi.org/10.1016/j.tafmec.2017.11.002.

Cao, R.H., Cao, P., Lin, H., Ma, G.W., Fan, X. and Xiong, X.G. (2018b), "Mechanical behavior of an opening in a jointed rock-like specimen under uniaxial loading: Experimental studies and particle mechanics approach", *Arch. Civ. Mech. Eng.,* **18**(1), 198-214. https://doi.org/10.1016/j.acme.2017.06.010.

Cao, R.H., Cao, P., Lin, H., Ma, G.W., Zhang, C.Y. and Jiang. C. (2018c), "Failure characteristics of jointed rock-like material containing multi-joints under a compressive-shear test: Experimental and numerical analyses", *Arch. Civ. Mech. Eng.,* **18**(3), 784-798. https://doi.org/10.1016/j.acme.2017.12.003.

Carlsson, J. and Isaksson, P. (2019), "Crack dynamics and crack tip shielding in a material containing pores analysed by a phase field method", *Eng. Fract. Mech.*, **206**, 526-540. https://doi.org/10.1016/j.engfracmech.2018.11.013.

Cho, N., Martin, C.D. and Sego, D.C. (2007), "A clumped particle model for rock", *Int. J. Rock Mech. Min. Sci.,* **44**(7), 997-1010.

Cox, B.N., Gao, H., Gross, D. and Rittel, D. (2005), "Modern topics and challenges in dynamic fracture", *J. Mech. Phys. Solids,* **53**(3), 565-596. https://doi.org/10.1016/j.ijrmms.2007.02.002.

Emdadi, A., Fahrenholtz, W.G., Hilmas, G.E. and Zaeem, M.A. (2018), "A modified phase-field model for quantitative simulation of crack propagation in single-phase and multi-phase materials", *Eng. Fract. Mech.,* **200**, 339-354. https://doi.org/10.1016/j.engfracmech.2018.07.038.

Fineberg, J., Gross, S.P., Marder, M. and Swinney, H.L. (1991), "Instability in dynamic fracture", *Phys. Rev. Lett.,* **67**(4), 457-460. https://doi.org/10.1103/PhysRevLett.67.457.

Fineberg, J. and Marder, M. (1999), "Instability in dynamic fracture", *Physiol. Rep.,* **313**(1-2), 1-108. https://doi.org/10.1016/S0370-1573(98)00085-4.

Fineberg, J. and Bouchbinder, E. (2015), "Recent developments in dynamic fracture: some perspectives", *Int. J. Fract.,* **196**(1-2), 33-57. https://doi.org/10.1007/s10704-015-0038-x.

Haeri, H., Sarfarazi, V., Zhu, Z., Hedayat, A., Nezamabadi, M.F. and Karbala M. (2018a), "Simulation of crack initiation and propagation in three point bending test using PFC2D", *Struct. Eng. Mech.,* **66**(4), 453-463. http://dx.doi.org/10.12989/sem.2018.66.4.453.

Haeri, H., Sarfarazi, V., Zhu, Z. and Lazemi, H.A. (2018b), "Investigation of the effects of particle size and model scale on the UCS and shear strength of concrete using PFC2D", *Struct. Eng. Mech.,* **67**(5), 505-516. http://dx.doi.org/10.12989/sem.2018.67.5.505.

Haeri, H., Sarfarazi, V., Zhu, Z. and Marji, M.F. (2018c), "Simulation of the tensile failure behaviour of transversally bedding layers using PFC2D", *Struct. Eng. Mech.,* **67**(5), 493-504. http://dx.doi.org/10.12989/sem.2018.67.5.493.

Haeri, H., Sarfarazi, V. and Zhu, Z. (2018d), "PFC3D simulation of the effect of particle size on the single edge-notched rectangle bar in bending test", *Struct. Eng. Mech.,* **68**(4), 497-505. http://dx.doi.org/10.12989/sem.2018.68.4.497.

Haeri, H., Sarfarazi, V. and Zhu, Z. (2018e), "Numerical simulation of the effect of bedding layer geometrical properties on the punch shear test using PFC3D", *Struct. Eng. Mech.,* **68**(4), 507-517. http://dx.doi.org/10.12989/sem.2018.68.4.507.

Hedjazi, L., Martin, C.L., Guessasma, S., Valle, G.D. and Dendievel, R. (2012), "Application of the Discrete Element Method to crack propagation and crack branching in a vitreous dense biopolymer material", *Int. J. Solids Struct.,* **49**(13), 1893-1899. https://doi.org/10.1016/j.ijsolstr.2012.03.030.

Kosteski, L., D'ambra, R. and Iturrioz, I. (2012), "Crack propagation in elastic solids using the truss-like discrete element method", *Int. J. Fract.,* **174**(2), 139-161. https://doi.org/10.1007/s10704-012-9684-4.

Martin, C.L., Bouvard, D. and Shima, S. (2003), "Study of particle rearrangement during powder compaction by the Discrete Element Method", *J. Mech. Phys. Solids,* **51**, 667-693. https://doi.org/10.1016/S0022-5096(02)00101-1.

Martin, C.L., Bouvard, D. and Delette, G. (2006), "Discrete element simulations of the compaction of aggregated ceramic powders", *J. Am. Ceram. Soc.,* **89**, 3379-3387. https://doi.org/10.1111/j.1551-2916.2006.01249.x.

Meng, Q.H. and Wang, Z.Q. (2015), "Numerical simulation of loading edge cracks by edge impact using the extended finite element method", *Acta Mech. Solida Sin.,* **28**(2), 156-167. https://doi.org/10.1016/S0894-9166(15)30004-5.

Meng, J., Cao, P., Huang, J., Lin, H., Chen, Y. and Cao, R. (2018), "Second-order cone programming formulation of discontinuous deformation analysis", *Int. J. Numer. Methods Eng.* https://doi.org/10.1002/nme.6006.

Miehe, C., Hofacker, M. and Welschinger, F. (2010a), "A phase field model for rate-independent crack propagation: Robust algorithmic implementation based on operator splits", *Comput. Methods Appl. Mech. Engrg.,* **199**(45-48), 2765-2778. https://doi.org/10.1016/j.cma.2010.04.011.

Miehe, C., Welschinger, F. and Hofacker, M. (2010b), "Thermodynamically consistent phase-field models of fracture: Variational principles and multi-field FE implementations", *Int. J. Numer. Meth. Engng.,* **83**(10), 1273-1311. https://doi.org/10.1002/nme.2861.

Mohammed, T.J., Bakar, B.H.A. and Bunnori, A.B. (2015), "Strengthening of reinforced concrete beams subjected to torsion with UHPFC composites", *Struct. Eng. Mech.,* **56**(1), 123-136. http://dx.doi.org/10.12989/sem.2015.56.1.123.

Nowruzpour, M., Sarkar, S., Reddy, J.N. and Roy, D. (2019), "A derivative-free upscaled theory for analysis of defects", *J. Mech. Phys. Solids,* **122**, 89-501. https://doi.org/10.1016/j.jmps.2018.09.018.

Nowruzpour, M. and Reddy, J.N. (2018), "Unification of local and nonlocal models within a stable integral formulation for analysis of defects", *Int. J. Eng. Sci.,* **132**, 45-59. https://doi.org/10.1016/j.ijengsci.2018.06.008.

Potyondy, D.O. and Cundall, P.A. (1998), "Modeling notch-formation mechanisms in the URL mine-by test tunnel using bonded assemblies of circular particles", *Int. J. Rock Mech. Min. Sci. Geomech. Abstr.,* **35**(4-5), 510-511. http://dx.doi.org/10.1016/2FS0148-9062(98)00083-7.

Potyondy, D.O. and Cundall, P.A. (2004), "A bonded-particle model for rock", *Int. J. Rock Mech. Min. Sci.,* **41**(8), 1329-1364. https://doi.org/10.1016/j.ijrmms.2004.09.011.

Procaccia, I. and Zylberg, J. (2013), "Propagation mechanism of brittle cracks", *Phys. Rev. E,* **87**, https://doi.org/10.1098/rspa.1964.0248.

Rabczuk, T., Song, J.H. and Belytschko, T. (2009), "Simulations of instability in dynamic fracture by the cracking particles method", *Eng. Fract. Mech.,* **76**(6), 730-741. https://doi.org/10.1016/j.engfracmech.2008.06.002.

Ravi-Chandar, K. and Knauss, W.G. (1984), "An experimental investigation into dynamic fracture: II. Microstructural aspects", *Int. J. Fract.,* **26**(1), 65-80. https://doi.org/10.1007/BF01152313.

Rosakis, A.J., Samundrala, O. and Coker D. (1999), "Cracks faster than the shear wave speed", *Science,* **284**, 1337-1340. https://doi.org/10.1126/science.284.5418.1337.

Sarfarazi, V. and Haeri, H. (2018), "Three-dimensional numerical modeling of effect of bedding layer on the tensile failure behavior in hollow disc models using Particle Flow Code (PFC3D)", *Struct. Eng. Mech.,* **68**(5), 537-547. https://doi.org/10.12989/sem.2018.68.5.537.

Sarkar, S., Nowruzpour, M., Reddy, J.N. and Srinivasa, S.A. (2017), "A discrete Lagrangian based direct approach to macroscopic modelling", *J. Mech. Phys. Solids,* **98**, 172-180. https://doi.org/10.1016/j.jmps.2016.09.007.

Sharon, E., Gross, S.P. and Fineberg, J. (1995), "Local crack branching as a mechanism for instability in dynamic fracture", *Phys. Rev. Lett.,* **74**(25), 5096-5099. https://doi.org/10.1103/PhysRevLett.74.5096.

Sharon, E. and Fineberg, J. (1999), "Confirming the continuum theory of dynamic brittle fracture for fast cracks", *Nature,* **397**(6717), 333-335. https://doi.org/10.1038/16891.

Shojaei, A., Mudric, T., Zaccariotto, M. and Galvanetto, U. (2016), "A coupled meshless finite point/Peridynamic method for 2D dynamic fracture analysis", *Int. J. Mech. Sci.,* **119**, 419-431. https://doi.org/10.1016/j.ijmecsci.2016.11.003.

Shojaei, A., Mossaiby, F., Zaccariotto, M. and Galvanetto, U. (2017), "The meshless finite point method for transient elastodynamic problems", *Acta Mech.* **228**(10), 3581-3593. https://doi.org/10.1007/s00707-017-1894-4.

Shojaei, A., Mossaiby F., Zaccariotto, M. and Galvanetto, U. (2018), "An adaptive multi-grid peridynamic method for dynamic fracture analysis", *Int. J. Mech. Sci.,* **144**, 600-617. https://doi.org/10.1016/j.ijmecsci.2018.06.020.

Shojaei, A., Galvanetto, U., Rabczuk, T., Jenabi, A. and Zaccariotto, M. (2019), "A generalized finite difference method based on the Peridynamic differential operator for the solution of problems in bounded and unbounded domains", *Comput. Methods Appl. Mech. Engrg.,* **343**, 100-126. https://doi.org/10.1016/j.cma.2018.08.033.

Song, J.H., Wang, H.W. and Belytschko, T. (2008), "A comparative study on finite element methods for dynamic fracture", *Comput. Mech.,* **42**(2), 239-250. https://doi.org/10.1007/s00466-007-0210-x.

Song, J.H. and Belytschko, T. (2009), "Cracking node method for dynamic fracture with finite elements", *Int. J. Numer. Methods Eng.,* **77**(3), 360-385. https://doi.org/10.1002/nme.2415.

Yang, Y.F., Li, G., Liang, Z.Z. and Tang, C.A. (2015), "Numerical investigation on crack branching during collision for rock-like material", *Theor. Appl. Fract. Mech.,* **76**, 35-49. https://doi.org/10.1016/j.tafmec.2014.12.010.

Zhang, P., Hu, X., Wang, X. and Yao, W. (2018), "An iteration scheme for phase field model for cohesive fracture and its implementation in Abaqus", *Eng. Fract. Mech.,* **204**, 268-287. https://doi.org/10.1016/j.engfracmech.2018.10.006.

Zhang, Z., and Chen, X. (2014), "Modeling nonlinear elastic solid with correlated lattice bond cell for dynamic fracture simulation", *Comput. Methods Appl. Mech. Engrg.,* **279**, 325-347. https://doi.org/10.1016/j.cma.2014.06.036.

CC